

# Laboratory Exploration of Heat Transfer Regimes in Rapidly Rotating Turbulent Convection

Jonathan S. Cheng,\* Matteo Madonia, Andrés J. Aguirre Guzmán, and Rudie P. J. Kunnen  
*Fluids & Flows group, Department of Applied Physics and J.M. Burgers Center for Fluid Dynamics,  
 Eindhoven University of Technology, P.O. Box 513, 5600 MB Eindhoven, Netherlands*

We report heat transfer and temperature measurements and direct numerical simulations of rapidly rotating convection in water. We achieve unprecedentedly strong rotational influence (Ekman numbers  $E$  as low as  $10^{-8}$ ). Scaling relations between the heat transfer (Nusselt number  $Nu$ ) and thermal forcing (Rayleigh number  $Ra$ ) demonstrate robust agreement with previous studies, extending those results further in parameter space. Examining the mid-height vertical temperature gradient reveals distinct regime changes of flow phenomenology, coinciding with transitions predicted by asymptotically-reduced simulations. We find a regime that we refer to as rotationally-influenced turbulence, inaccessible to asymptotics, where rotation is important but not as dominant as in the known geostrophic turbulence regime. The temperature gradients for all  $E$  values collapse to a  $Ra^{-1/3}$  scaling in this new regime.

Convectively driven, rotationally constrained flows form the basis of many geophysical processes, from dynamo action in the molten iron core of the Earth [1] to atmospheric patterns in gas giants [2]. These systems are massive and complex, such that our understanding of their flows depends on greatly simplified models. Much can be learned by distilling the physics down to the canonical problem of rotating Rayleigh-Bénard convection, where a layer of fluid is subject to an unstable vertical temperature gradient and rotates about a vertical axis. Even in this reduced problem, though, vastly different flows emerge depending on the relative strength of rotational and convective forces, and it is imperative that their properties are understood before extrapolating to geophysical settings. Though rotating convection is well-studied at moderate degrees of thermal forcing and rotation in laboratory experiments [3–6] and direct numerical simulations (DNS) [7, 8], a massive parameter gap separates such studies from the extreme conditions of planets [9, 10].

Recent studies aiming to bridge this parameter gap have employed large-scale experimental setups [11–14] and high resolution simulations [12, 15–17]. Though gains may appear marginal in the geophysical context, these studies have, in fact, manifested a plethora of novel behaviors not previously observed. Of particular interest is the range where thermal forcing and rotation both strongly affect the system but neither dominates the other, the so-called “geostrophic turbulence” (GT) regime. Parameter estimates for conditions in planetary fluid layers indicate that understanding GT may be the crux to determining how rotating convection models relate to geophysical systems [14, 18].

Rotating convection regimes are often characterized by relationships between the heat transfer parameters.

The Rayleigh number,  $Ra = \alpha_T g \Delta T H^3 / \nu \kappa$ , describes the magnitude of thermal forcing, where  $\alpha_T$  is the coefficient of thermal expansion,  $g$  is gravitational acceleration,  $\Delta T$  is the temperature difference between upper and lower boundaries,  $H$  is the height of the fluid layer,  $\nu$  is the kinematic viscosity, and  $\kappa$  is the thermal diffusivity. Fig. 1a & b visualize the turbulent flows at high  $Ra$  achieved in our experiments. Increasing  $Ra$  leads to correspondingly smaller-scale flow structures. The Nusselt number,  $Nu = qH/k\Delta T$ , describes the heat transfer efficiency of the system, where  $q$  is the applied heat flux and  $k$  is the thermal conductivity of the fluid.  $Nu = 1$  indicates pure thermal conduction while  $Nu > 1$  indicates the presence of convective heat transport. The Prandtl number  $Pr = \nu/\kappa$ , describing the material properties of the fluid, is often fixed at 1 or near 1 in extreme simulations and experiments [13], but can range from  $\sim 0.1$  to 10 in geophysical settings [9]. The heat transfer efficiency forms a power law relationship with the thermal forcing such that  $Nu \sim Ra^\gamma$ , with distinct values of  $\gamma$  corresponding to distinct behavioral regimes [19, 20].

Rotational influence is represented by the Ekman number  $E = \nu/2\Omega H^2$ , where  $\Omega$  is the angular frequency and lower  $E$  corresponds to greater rotational constraint. The convective Rossby number  $Ro = (RaE^2/Pr)^{1/2}$  is used to compare rotational and convective forces: traditionally,  $Ro \lesssim 1$  is “rotationally-affected” while  $Ro \gtrsim 1$  is “rotationally-unaffected” [21, 22]. Rotation contributes a vertical ‘stiffness’ to the flow, suppressing the onset of stationary convection to  $Ra_C = 8.7E^{-4/3}$  [23] and to the form of cellular structures with horizontal scale  $\ell_\nu \sim E^{1/3}H$  [24, 25]. Analogous to nonrotating convection,  $Nu$  vs.  $Ra/Ra_C$  scaling relationships indicate distinct behavioral regimes.

As visualized in our experiments (see Fig. 1c–f), the dominant flow structures evolve as  $Ra$  increases relative to  $Ra_C$ . Much of our intuition for these structures comes from simulations of the asymptotically-reduced equa-

\* Current affiliation: Department of Mechanical Engineering, University of Rochester, Rochester, NY 14627, USA

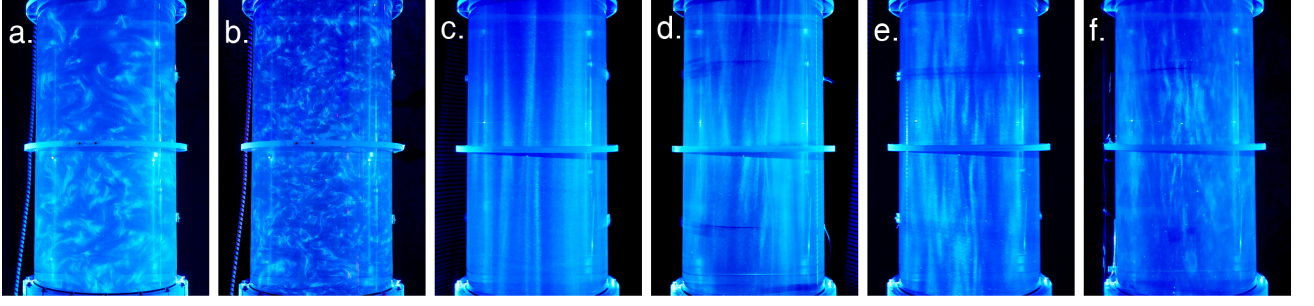


FIG. 1. Visualizations of the flow field in a vertical slice of the  $\Gamma = 1/5$  tank. Panels a & b: nonrotating convection at  $Ra =$  a)  $1.4 \times 10^{11}$ , b)  $2.2 \times 10^{12}$ . Panels c–f: rotating convection at  $E = 5 \times 10^{-8}$  and  $Ra =$  c)  $9.6 \times 10^{10}$  (convective Taylor columns), d)  $8.6 \times 10^{11}$  (convective plumes), e)  $1.6 \times 10^{12}$  (geostrophic turbulence), f)  $3.3 \times 10^{12}$  (rotationally-influenced turbulence). The photos are captured by seeding the water with neutrally buoyant rheoscopic particles [26] and illuminating it with a vertical light sheet.

tions, a set of equations rescaled in the limit of infinitely rapid rotation such that  $E, Ro \rightarrow 0$  [27]. In the context of asymptotic simulations [18, 28],  $Ra/Ra_C$  values correspond to “convective Taylor columns” (panel c) where narrow structures span the tank vertically, “convective plumes” (panel d) where the columns begin to laterally interact and become wavy, and GT (panel e), the aforementioned regime where convective forces have destroyed the columnar structure but flows are still constrained to rotational length scales. GT at low  $E$  ( $\lesssim 10^{-6}$ ) exists at the limit of accessibility for asymptotic simulations and DNS; it remains largely uncharacterized at  $Pr > 1$  and with poorly constrained scaling properties even at  $Pr \simeq 1$  [13, 16, 17, 28].

The onset horizontal scale  $\ell_\nu$  is believed to accurately describe flows in Fig. 1c–e, and serves as a necessary condition for closure of the asymptotically-reduced equations [27]. This assumption persists until a theoretical upper bound, beyond which buoyancy takes over the horizontal length scale [29, 30]:

$$Ra \sim E^{-8/5} Pr^{3/5}. \quad (1)$$

The final image (panel f) in Fig. 1 lies beyond this upper bound, demonstrating clear differences in flow morphology and setting up another open question: Flows in the realm of  $Ro \lesssim 1$  are well-studied at moderate  $E$ , but, much as in GT, the behaviors in this range change fundamentally as  $E$  decreases. For example, an overshoot in  $Nu$  above the nonrotating value is well-documented here [6, 22], but vanishes for  $E \lesssim 10^{-6}$ , with  $Nu$  being suppressed at even lower  $E$  [14]. How do we characterize the flows in this range – which we refer to as “rotationally-influenced turbulence” (RIT) – when we lack asymptotic simulations to guide our predictions?

In this study, we analyze 75 new nonrotating and rotating convection data points from the TROCONVEX laboratory setup and from direct numerical simulations, over parameter ranges  $10^{10} < Ra < 10^{14}$  and  $10^{-8} \leq E \leq 3 \times 10^{-7}$ . These data extend the upper bound of  $Ra$  by a decade and the lower bound of  $E$  by factor of three

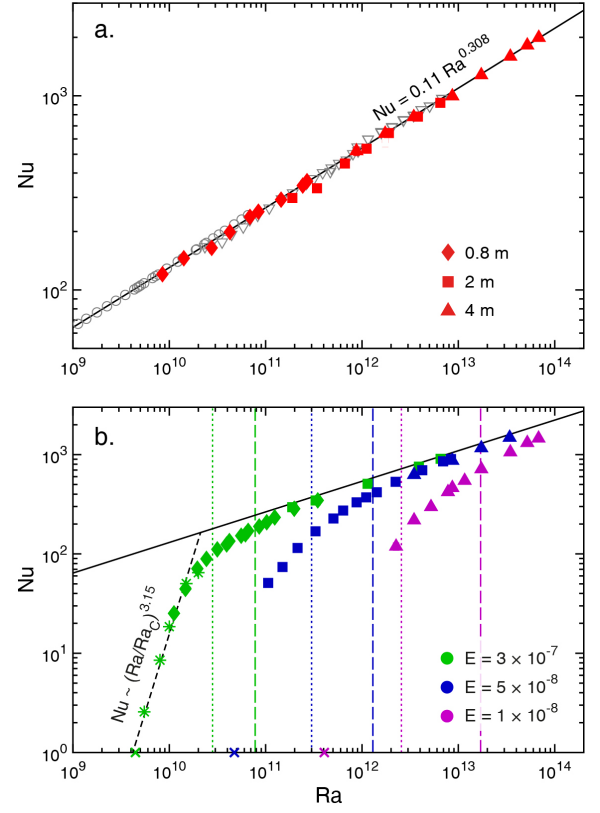


FIG. 2. Nusselt number ( $Nu$ ) plotted versus Rayleigh number ( $Ra$ ) for nonrotating convection (panel a) and rotating convection (panel b) experiments. In both panels, the marker shape represents tank height  $H$  and the solid line represents our best-fit nonrotating convection trend ([? ]). The associated aspect ratios for different heights are  $\Gamma = 1/2$  for  $H = 0.8$  m (diamonds),  $\Gamma = 1/5$  for  $H = 2$  m (squares), and  $\Gamma = 1/10$  for  $H = 4$  m (triangles). Data from previous studies are included as open grey circles [31] and triangles [14]. In panel b, color represents the Ekman number ( $E$ ).  $Ra_C$  in each case is indicated by ‘x.’ Numerical simulations at  $E = 3 \times 10^{-7}$  are shown as asterisks. Dotted lines represent the predicted transition from convective columns to plumes in [32], while dashed lines represent the predicted transition from geostrophic turbulence to rotationally-influenced turbulence. A best-fit line through the steep region at  $E = 3 \times 10^{-7}$  follows  $Nu \sim (Ra/Ra_C)^{3.15}$ .

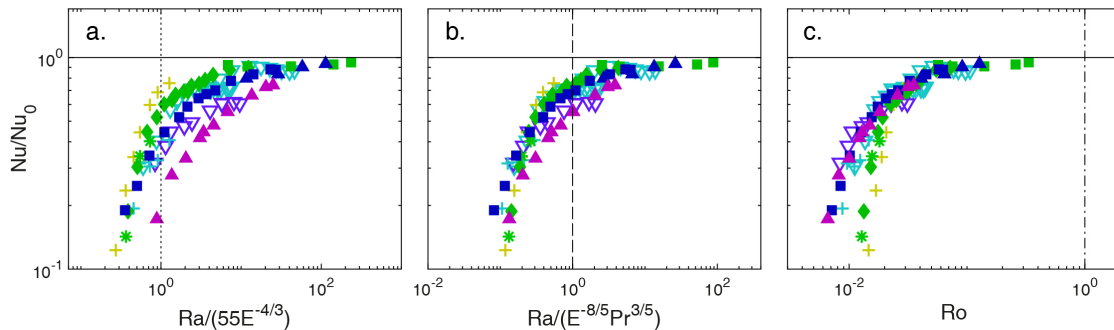


FIG. 3.  $Nu$  compensated by nonrotating scaling (2) versus  $Ra$  compensated by a)  $Ra \sim 55E^{-4/3}$  [32], b)  $Ra \sim E^{-8/5}Pr^{3/5}$  [29], and c)  $Ra \sim E^{-1}Pr^{1/2}$  ( $Ro = 1$ ) [21]. Bullet color and shape are the same as in Fig. 2, with additional points from [14]: Numerical  $E = 1 \times 10^{-6}$  cases are yellow crosses, numerical  $E = 1 \times 10^{-7}$  cases are cyan crosses, laboratory  $E \simeq 10^{-7}$  cases are empty cyan triangles, and laboratory  $E \simeq 3 \times 10^{-8}$  cases are empty indigo triangles.

compared to previous  $Pr > 1$  studies. Consistent scaling trends in  $Nu$  vs.  $Ra$  are observed over a broad range of aspect ratios and between DNS and laboratory experiments, including close agreement with previous work. Near-onset cases undergoing cellular and columnar convection [Fig. 1c] correspond to a steep  $Nu$ – $Ra$  scaling, cases far from onset in the RIT regime [Fig. 1f] approach the shallow nonrotating scaling, and in-between cases (plumes, GT) [Fig. 1d & e] follow an intermediate scaling. In contrast to previous work, no single transition scaling is found to collapse all data.

The reason for this becomes clear when we examine the mean vertical temperature gradient  $\partial_z \bar{T}$  across the mid-plane ( $z = 0.5$ ). When plotted against  $Ra/Ra_C$ , the temperature gradient undergoes distinct reversals in trend, marking flow regime transitions in a far clearer way than tracking the  $Nu$ – $Ra$  scaling  $\gamma$ . The locations of these reversals correspond closely with transition predictions from asymptotic studies, and they notably spread apart as  $E$  decreases – a behavior that cannot be captured by any single transition scaling. GT manifests as a saturation in the temperature gradient [28] whose parameter range expands as  $E$  decreases, and subsequently transitions into RIT in a location that coincides precisely with (1). Scaling  $Ra$  by (1) collapses temperature gradient data across all  $E$  values into a single trend, indicating a previously unobserved, but robust mode of heat transport in this regime.

Laboratory data are acquired from TROCONVEX: a large-scale rotating convection device at Eindhoven University of Technology. In order to access broad ranges of  $Ra$  and  $E$ , interchangeable tanks of height  $H = 0.8, 2$ , and  $4$  m but equal diameter  $D = 0.39$  m are used. Temperatures are measured via thermistors embedded in the top, bottom, and sidewall of these tanks. Top and bottom thermistors give the overall temperature gradient for calculating the globally-averaged parameters  $Nu$  and  $Ra$ , while sidewall thermistors measure vertical temperature profiles. Further details are in the Supplement [33]. The working fluid is water at a mean temperature of around

31°C, corresponding to  $Pr = 5.2$ . Numerical simulations bridge the gap between laboratory data and the onset of convection, where the minute temperature differences required cannot be stably maintained in the lab [12, 34]. DNS runs are conducted at  $E = 3 \times 10^{-7}$ ,  $Pr = 5.5$  in a  $384 \times 384 \times 640$  cell cartesian grid of aspect ratio  $\Gamma = 10\ell_\nu/H = 0.323$  (horizontal dimensions are each of size  $10\ell_\nu$ ). The temperature field is resolved on a grid refined by a factor of 2 in both horizontal directions. Non-slip and constant-temperature conditions apply at the top and bottom boundaries, while horizontal boundary conditions are periodic. Further details about the code are in [35]. All experimental and numerical data are tabulated in the Supplement [33].

Fig. 2 shows our data in terms of  $Nu$  versus  $Ra$  values. Nonrotating data [Fig. 2a] follow a best-fit scaling of

$$Nu_0 = 0.11 \left( {}^{+0.02}_{-0.01} \right) Ra^{0.308 \pm 0.005}, \quad (2)$$

agreeing with previous scaling trends of  $\sim 0.3 - 0.33$  found in water [14, 36, 37] and in other media [38–40]. It is also consistent with the classical prediction  $Nu \sim Ra^{1/3}$  where the bulk is sufficiently turbulent as to be approximately isothermal, with the temperature gradient confined to the upper and lower thermal boundary layers [19]. There is no evidence of a transition to a steeper scaling that would indicate the ultimate regime of RBC [20, 41], though this may be because of the narrow geometry employed ( $\Gamma \leq 1/2$ ). Rotating data [Fig. 2b] follow a characteristically steep slope near onset which flattens toward the nonrotating scaling (2) as  $Ra/Ra_C$  increases. For  $E = 3 \times 10^{-7}$ , we observe robust agreement between simulations and laboratory experiments. Plotting a best-fit trend in the cellular and columnar regimes gives  $Nu \sim (Ra/Ra_C)^{3.15 \pm 0.15}$ , consistent with scalings found in other low- $E$ ,  $Pr \simeq 3$ – $10$  studies [12, 14, 16]. As is characteristic for low  $E$ , rotational  $Nu$  values lie below the nonrotating  $Nu_0$  values until well beyond onset. This separation becomes more pronounced as  $E$  decreases: the  $E = 3 \times 10^{-7}$  trend first comes within 10% of the non-

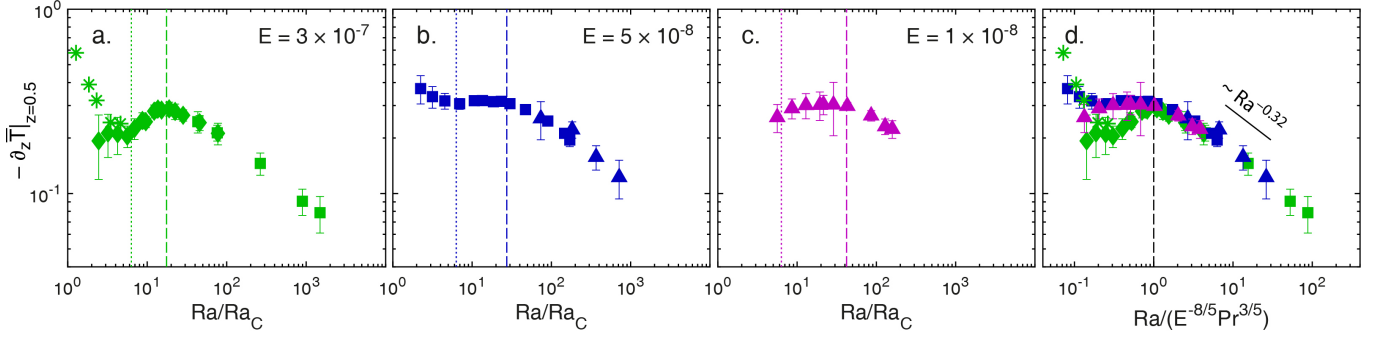


FIG. 4. Normalized mid-height temperature gradient  $-\partial_z \bar{T}|_{z=0.5}$  plotted versus  $Ra/Ra_C$  for a)  $E = 3 \times 10^{-7}$ , b)  $E = 5 \times 10^{-8}$ , and c)  $E = 1 \times 10^{-8}$ . Symbol shapes correspond to tank aspect ratio, as in Fig. 2. Dotted lines represent Eq. (3); dashed lines Eq. (1). d) Normalized mid-height temperature gradient  $-\partial_z \bar{T}|_{z=0.5}$  plotted versus  $Ra$  compensated by (1) for data at all three  $E$  values combined. A best-fit scaling across all  $E$  values beyond the transition produces a trend of  $-\partial_z \bar{T}|_{z=0.5} \sim Ra^{-0.32}$ .

rotating trend at  $Ra/Ra_C = 43$ , while for  $E = 5 \times 10^{-8}$  this does not occur until  $Ra/Ra_C = 370$ . This seems to indicate that the range of GT expands as  $E$  is lowered, although predicted regime transitions (marked by dotted and dashed lines in Fig. 2b) only roughly map out changes in the  $Nu$ - $Ra$  scaling.

This smoothness is further evident in Fig. 3, where  $Nu$  is compensated by the best-fit nonrotating trend  $Nu_0$  (2), and  $Ra$  is compensated by several transition arguments. In contrast to previous studies, it is unclear whether any of these arguments definitively collapse data over multiple  $E$  values [13, 14]. Fig. 3a compensates  $Ra$  by an asymptotic prediction for the transition from columnar convection to plumes [32]:

$$Ra = 55E^{-4/3}, \quad (3)$$

but gives little evidence of collapse. Compensating with (1) collapses the near-onset trends while inducing some spread in the GT range [Fig. 3b], while compensating by  $Ro$  does the opposite [Fig. 3c]. In Fig. 3c, it can be seen that all data reside well before the  $Ro_C = 1$  transition marking the onset of nonrotating-style convection [21, 22]. The visualization in Fig. 1f confirms that rotational effects are still felt by the flow when  $Nu$  approaches  $Nu_0$ , but the gradual shifts in  $Nu$  do little to characterize the flow physics.

In lieu of detailed transition information from the globally-averaged parameters, we turn our focus to the mean vertical temperature gradient  $-\partial_z \bar{T}|_{z=0.5}$ . In non-rotating convection, the temperature profile is sharply divided between the bulk, which is nearly isothermal ( $-\partial_z \bar{T} \approx 0$ ), and the thermal boundary layers, within which nearly all of the temperature drop  $\Delta T$  occurs [20, 42]. In rotating convection, however, the shape of the temperature profile evolves as  $Ra/Ra_C$  increases and the flow morphology changes. The portion of the temperature gradient partitioned to the bulk likewise evolves, giving it diagnostic properties [17, 28, 32].

Fig. 4a-c show that the temperature gradient measured at tank mid-height,  $-\partial_z \bar{T}|_{z=0.5}$ , is indeed a robust tool for determining regime transitions at each  $E$  value (information on how  $-\partial_z \bar{T}|_{z=0.5}$  and associated error bars are calculated from raw temperature data can be found in the Supplement [33]). In the cellular and columnar regimes, increasing  $Ra$  leads to a decreasing temperature gradient. At (3) this trend reverses, indicating that increasing  $Ra$  now forces more of the temperature gradient into the interior as the horizontal rigidity of bulk flow structures relaxes. Visualizations of the flow and  $Nu$ - $Ra$  data do not make it clear where the plumes-GT regime transition takes place. However, asymptotic studies posit that GT corresponds to  $-\partial_z \bar{T}|_{z=0.5}$  flattening with increasing  $Ra/Ra_C$  [28]. Qualitatively, our results do appear to manifest such a flattening at  $Ra/Ra_C \simeq 15$  at each  $E$  value. This abruptly gives way to a decreasing trend at (1), where the flow enters the RIT regime. As (1) and (3) are separated by a factor of  $E^{4/15}$ , the parameter range of GT evidently increases as  $E$  decreases toward geophysical values.

In Fig. 4d we plot  $-\partial_z \bar{T}|_{z=0.5}$  data for all  $E$  values versus  $Ra$  rescaled by (1). All data to the right of the dashed line, then, lie in RIT. Overplotting separate  $E$  trends collapses all data in this regime into an approximate  $-\partial_z \bar{T}|_{z=0.5} \sim Ra^{-1/3}$  scaling. We speculate that nonrotating-style thermal boundary layers have formed beyond this transition, such that increasing  $Ra$  causes stronger mixing in the bulk and isolates more of the temperature gradient into the boundary layers. This scaling exponent is, to the best of our knowledge, a novel result in rotating convection, and the fact that it has not been observed in higher  $E$  ranges reinforces the idea that the traditional understanding of the “rotationally-affected” regime no longer applies to its low- $E$  analogue, the RIT regime.

Our novel rotating convection survey demonstrates the emergence of several distinct regimes as  $E$  is pushed lower than any previous study in water. The  $Nu$ - $Ra$

scaling exponent  $\gamma$  demonstrates consistency with previous results while extending them to more extreme parameters, but has limited utility in determining precise transition locations. The mid-height temperature gradient  $-\partial_z \bar{T}|_{z=0.5}$  provides a robust measure in this regard: transitions that are nigh invisible in  $Nu-Ra$  plots [Figs. 2 & 3] are expressed as distinctive reversals in the  $-\partial_z \bar{T}|_{z=0.5}$  vs.  $Ra/Ra_C$  trend [Fig. 4]. With this method, we confirm that the GT range expands as  $E$  decreases. We also encounter the presence of an RIT regime for  $Ra > E^{-8/5} Pr^{3/5}$ , analogous to the rotationally-affected regime of moderate  $E$  [6, 22], but containing novel behaviors. Here, data over all  $E$  values collapse as  $-\partial_z \bar{T}|_{z=0.5} \sim Ra^{-1/3}$ . This decreasing trend expresses how thermal gradients are funneled into the boundary layers with increasing  $Ra$ .

Our results clarify that GT is not the only intermediate regime separating “rotationally-dominated” convection from nonrotating-style turbulence; in fact, the apparent majority of parameter space prior to  $Ro \sim 1$  is occupied by RIT. If we extrapolate the asymptotic arguments supported in this paper, the spaces between each transition widen as  $E$  decreases: the plumes / GT range expands as  $Ra \sim E^{4/15}$  while the RIT range expands as  $Ra \sim E^{2/5}$ . Estimates for planetary fluid layers give  $E \sim 10^{-19} - 10^{-12}$  [9] and  $Ra/Ra_C \sim 10^2 - 10^3$  [43]. Rotating convection in these layers would then invariably inhabit either geostrophic turbulence or rotationally-influenced turbulence. Though this analysis is certainly too simplistic to capture the complexity of planetary flows, it reinforces that the relevant physics are not likely present in classical rotating convection models. This work provides a significant step toward developing new models for geophysically-relevant regimes of rotating convection.

The authors have received funding from the European Research Council (ERC) under the European Union’s Horizon 2020 research and innovation programme (Grant agreement No. 678634). We are grateful for the support of the Netherlands Organisation for Scientific Research (NWO) for the use of supercomputer facilities (Cartesius) under Grants No. 15462, 16467 and 2019.005.

---

[1] G. A. Glatzmaier and P. H. Roberts, *Phys. Earth Planet. Inter.* **91**, 63 (1995).  
[2] M. Heimpel, J. Aurnou, and J. Wicht, *Nature* **438**, 193 (2005).  
[3] H. T. Rossby, *J. Fluid Mech.* **36**, 309 (1969).  
[4] Y. Liu and R. E. Ecke, *Phys. Rev. Lett.* **79**, 2257 (1997).  
[5] R. P. J. Kunnen, H. J. H. Clercx, and B. J. Geurts, *EPL (Europhysics Letters)* **84**, 24001 (2008).  
[6] J.-Q. Zhong, R. J. A. M. Stevens, H. J. H. Clercx, R. Verzicco, D. Lohse, and G. Ahlers, *Phys. Rev. Lett.* **102**, 044502 (2009).  
[7] K. Julien, S. Legg, J. McWilliams, and J. Werne, *J. Fluid Mech.* **322**, 243 (1996).

[8] S. Schmitz and A. Tilgner, *Phys. Rev. E* **80** (2009).  
[9] G. Schubert and K. M. Soderlund, *Phys. Earth Planet. Inter.* **187**, 92 (2011).  
[10] P. H. Roberts and E. M. King, *Rev. Prog. Phys.* **76**, 096801 (2013).  
[11] S. Weiss and G. Ahlers, *J. Fluid Mech.* **684**, 407 (2011).  
[12] E. M. King, S. Stellmach, and J. M. Aurnou, *J. Fluid Mech.* **691**, 568 (2012).  
[13] R. E. Ecke and J. J. Niemela, *Phys. Rev. Lett.* **113**, 114301 (2014).  
[14] J. S. Cheng, S. Stellmach, A. Ribeiro, A. Grannan, E. M. King, and J. M. Aurnou, *Geophys. J. Int.* **201**, 1 (2015).  
[15] B. Favier, L. J. Silvers, and M. R. E. Proctor, *Phys. Fluids* **26**, 096605 (2014).  
[16] S. Stellmach, M. Lischper, K. Julien, G. Vasil, J. S. Cheng, A. Ribeiro, E. M. King, and J. M. Aurnou, *Phys. Rev. Lett.* **113**, 254501 (2014).  
[17] R. P. J. Kunnen, R. Ostilla-Mónico, E. P. van der Poel, R. Verzicco, and D. Lohse, *J. Fluid Mech.* **799**, 413 (2016).  
[18] J. M. Aurnou, M. A. Calkins, J. S. Cheng, K. Julien, E. M. King, D. Nieves, K. M. Soderlund, and S. Stellmach, *Phys. Earth Planet. Inter.* **246**, 52 (2015).  
[19] W. V. Malkus, *Proc. Roy. Soc. Lond. A* **225**, 196 (1954).  
[20] G. Ahlers, S. Grossmann, and D. Lohse, *Rev. Mod. Phys.* **81**, 503 (2009).  
[21] P. A. Gilman, *Geophys. Astrophys. Fluid Dyn.* **8**, 93 (1977).  
[22] R. J. A. M. Stevens, H. J. H. Clercx, and D. Lohse, *Eur. J. Mech. B/Fluids* **40**, 41 (2013).  
[23] S. Chandrasekhar, *Hydrodynamic and Hydromagnetic Stability*, 1st ed. (Oxford University Press, 1961).  
[24] K. Zhang and G. Schubert, *Ann. Rev. Fluid Mech.* **32**, 409 (2000).  
[25] S. Stellmach and U. Hansen, *Phys. Rev. E* **70**, 056312 (2004).  
[26] D. Borrero-Echeverry, C. J. Crowley, and T. P. Riddick, *Phys. Fluids* **30**, 087103 (2018).  
[27] M. Sprague, K. Julien, E. Knobloch, and J. Werne, *J. Fluid Mech.* **551**, 141 (2006).  
[28] K. Julien, A. M. Rubio, I. Grooms, and E. Knobloch, *Geophys. Astrophys. Fluid Dyn.* **106**, 254503 (2012).  
[29] K. Julien, E. Knobloch, A. M. Rubio, and G. M. Vasil, *Phys. Rev. Lett.* **109**, 254503 (2012).  
[30] T. Gastine, J. Wicht, and J. Aubert, *J. Fluid Mech.* **808**, 690 (2016).  
[31] D. Funfschilling, E. Brown, A. Nikolaenko, and G. Ahlers, *J. Fluid Mech.* **536**, 145 (2005).  
[32] D. Nieves, A. M. Rubio, and K. Julien, *Phys. Fluids* **26**, 086602 (2014).  
[33] See Supplemental Material at [url], which includes Refs. [44–50], for description of the experimental apparatus, measurement techniques, error analysis, additional figures, and data tables.  
[34] J. S. Cheng, J. M. Aurnou, K. Julien, and R. P. J. Kunnen, *Geophys. Astrophys. Fluid Dyn.* **112**, 277 (2018).  
[35] R. Ostilla-Mónico, Y. Yang, E. P. van der Poel, D. Lohse, and R. Verzicco, *J. Comput. Phys.* **301**, 308 (2015).  
[36] E. Brown, A. Nikolaenko, D. Funfschilling, and G. Ahlers, *Phys. Fluids* **17**, 075108 (2005).  
[37] C. Sun, L.-Y. Ren, H. Song, and K.-Q. Xia, *J. Fluid Mech.* **542**, 165 (2005).  
[38] J. J. Niemela, L. Skrbek, K. R. Sreenivasan, and R. J. Donnelly, *Nature* **404**, 837 (2000).

- [39] D. Funfschilling, E. Bodenschatz, and G. Ahlers, Phys. Rev. Lett. **103**, 014503 (2009).
- [40] J. J. Niemela, S. Babuin, and K. R. Sreenivasan, J. Fluid Mech. **649**, 509 (2010).
- [41] R. H. Kraichnan, Phys. Fluids **5**, 1374 (1962).
- [42] S. Grossmann and D. Lohse, J. Fluid Mech. **407**, 27 (2000).
- [43] J. S. Cheng and J. M. Aurnou, Earth Planet. Sci. Lett. **436**, 121 (2016).
- [44] G. V. Bayley and J. M. Hammersley, J. R. Stat. Soc. Suppl. **8**, 184 (1946).
- [45] J. Taylor, *Introduction to Error Analysis, The Study of Uncertainties in Physical Measurements*, 2nd ed. (University Science Books, 1997).
- [46] D. R. Lide, *CRC Handbook of Chemistry and Physics: A Ready-Reference Book of Chemical and Physical Data: 2003–2004* (CRC Press, 2003).
- [47] E. Brown and G. Ahlers, Europhys. Lett. **80**, 14001 (2007).
- [48] R. P. J. Kunnen, B. J. Geurts, and H. J. H. Clercx, J. Fluid Mech. **642**, 445 (2010).
- [49] A. Zięba and P. Ramza, Metrol. Meas. Syst. **18**, 529 (2011).
- [50] S. Horn and J. M. Aurnou, Phys. Rev. Fluids **4**, 073501 (2019).